

# The Polarization of Scattered Ly $\alpha$ Radiation Around High-Redshift Galaxies

Mark Dijkstra<sup>\*</sup> and Abraham Loeb<sup>†</sup>

*Harvard-Smithsonian Center for Astrophysics, 60 Garden Street, Cambridge, MA 02138, USA*

3 May 2019

## ABSTRACT

The high-redshift Universe contains luminous Ly $\alpha$  emitting sources such as galaxies and quasars. The emitted Ly $\alpha$  radiation is often scattered by surrounding neutral hydrogen atoms. We show that the scattered Ly $\alpha$  radiation obtains a high level of polarization for a wide range of likely environments of high-redshift galaxies. For example, the back-scattered Ly $\alpha$  flux observed from galaxies surrounded by a superwind-driven outflow may reach a fractional polarization as high as  $\sim 40\%$ . Equal levels of polarization may be observed from neutral collapsing protogalaxies. Resonant scattering in the diffuse intergalactic medium typically results in a lower polarization amplitude ( $\lesssim 7\%$ ), which depends on the flux of the ionizing background. Spectral polarimetry can differentiate between Ly $\alpha$  scattering off infalling gas and outflowing gas; for an outflow the polarization should increase towards longer wavelengths while for infall the opposite is true. Our numerical results suggest that Ly $\alpha$  polarimetry is feasible with existing instruments, and may provide a new diagnostic of the distribution and kinematics of neutral hydrogen around high-redshift galaxies. Moreover, polarimetry may help suppress infrared lines originating in the Earth's atmosphere, and thus improve the sensitivity of ground-based observations to high-redshift Ly $\alpha$  emitting galaxies outside the currently available redshift windows.

**Key words:** cosmology: theory–galaxies: high redshift–line: formation–polarization–scattering

## 1 INTRODUCTION

The Lyman- $\alpha$  (Ly $\alpha$ ) line serves as an excellent tracer of high-redshift galaxies and quasars (e.g. Partridge & Peebles 1967; Hu & McMahon 1996; Steidel et al. 1996; Trager et al. 1997; Rhoads et al. 2000; Hu et al. 2002; Kodaira et al. 2003; Kashikawa et al. 2006; Tapken et al. 2006; Westra et al. 2006; Stanway et al. 2007; Ouchi et al. 2007; Rauch et al. 2007). Searches for redshifted Ly $\alpha$  emission have discovered galaxies robustly out to redshifts  $z = 6.96$  (Iye et al. 2006), and potentially out to  $z = 10$  (Stark et al. 2007a). These observations provide a unique glimpse into galaxy formation at high-redshift (Malhotra & Rhoads 2002; Dijkstra & Wyithe 2007), and into the Epoch of Reionization (EoR, e.g. Loeb & Rybicki 1999; Haiman & Spaans 1999; Malhotra & Rhoads 2004; Haiman & Cen 2005; Dijkstra et al. 2007a; Stark et al. 2007b; McQuinn et al. 2007; Ota et al. 2007; Kobayashi et al. 2007; Fernandez & Komatsu 2007; Mesinger & Furlanetto 2007). Future surveys intend to

exploit this window further by pushing to even higher redshifts and fainter flux levels (e.g. Stark et al. 2007b; Nilsson et al. 2007, and references therein).

The interpretation of existing and future observations is complicated by the fact that Ly $\alpha$  photons are typically scattered both in the interstellar medium (ISM, e.g. Hansen & Oh 2006) as well as in the intergalactic medium (IGM, Loeb & Rybicki 1999; Santos 2004; Dijkstra et al. 2007). The impact of scattering on the observed Ly $\alpha$  flux and spectrum may be derived by careful modeling of the observed Ly $\alpha$  line profile, combined with constraints on the galaxy's stellar population derived from its broad band colors (Verhamme et al. 2006, 2008). Also, observations of the Ly $\alpha$  line in local starburst galaxies can shed light on the processes that regulate the transfer and escape of Ly $\alpha$  from star forming galaxies (Kunth et al. 1998; Hayes et al. 2007). Of course, it is not obvious whether local starburst galaxies are representative of high-redshift Ly $\alpha$  emitters (LAEs), and detailed modeling of the line profile may be hampered by the quality of the data of high-redshift LAEs.

In this paper, we describe a complementary approach to studying the environments of high-redshift LAEs, which involves the polarization properties of the scattered Ly $\alpha$

<sup>\*</sup> E-mail:mdijkstr@cfa.harvard.edu

<sup>†</sup> E-mail:aloeb@cfa.harvard.edu

radiation. In the context of the solar system, the polarization of resonantly scattered Ly $\alpha$  photons from the sun by neutral hydrogen in the interplanetary medium and in the Earth's atmosphere has been studied extensively (e.g. Brandt & Chamberlain 1959), occasionally by using a Monte-Carlo method to compute the Ly $\alpha$  radiative transfer (Modali et al. 1972; Keller et al. 1981). In the cosmological context, Lee & Ahn (1998) showed that Ly $\alpha$  emerging from an unresolved star-bursting galaxy may be polarized to a considerable level ( $\sim 5\%$ ), and Rybicki & Loeb (1999) showed that scattering of Ly $\alpha$  photons from a point source embedded in the Hubble flow of a neutral IGM would produce a polarized Ly $\alpha$  halo around the source. Despite the emergence of several Monte-Carlo Ly $\alpha$  radiative transfer codes in recent years (e.g. Zheng & Miralda-Escudé 2002; Cantalupo et al. 2005; Tasitsiomi 2006; Dijkstra et al. 2006; Verhamme et al. 2006; Laursen & Sommer-Larsen 2007; Semelin et al. 2007), the polarization properties of scattered Ly $\alpha$  photons around galaxies have not been investigated in a broader context beyond this early work.

The goal of this paper is to demonstrate that Ly $\alpha$  radiation may be highly polarized around high-redshift galaxies in a broad range of cosmological circumstances. We will show that Ly $\alpha$  polarimetry may place constraints on the kinematics of the gas through which the photons propagate. This is important: understanding the impact of scattering in both the ISM and IGM on the observed Ly $\alpha$  properties is required to fully exploit Ly $\alpha$  observations as a probe of the high-redshift Universe. Furthermore, we discuss the possibility of separating Ly $\alpha$  sources from low-redshift line emitters (such as [OII], [OIII], H $\alpha$ , H $\beta$  emitters, and OH-skylines) based on polarimetry.

The outline of this paper is as follows: In § 2 we describe the basic principles of Ly $\alpha$  radiative transfer and polarization, and how polarization is incorporated in our radiative transfer calculations. In § 3 we present our main numerical results. In § 4 we discuss our results and their implications, before presenting our final conclusions in § 5. The parameters for the background cosmology used throughout this paper are  $(\Omega_m, \Omega_\Lambda, h) = (0.24, 0.76, 0.73)$  (Spergel et al. 2007).

## 2 LY $\alpha$ SCATTERING & POLARIZATION

### 2.1 Ly $\alpha$ Radiative Transfer Basics

We start by summarizing the basic principles of Ly $\alpha$  scattering. We express photon frequency  $\nu$  in terms of a dimensionless variable  $x \equiv (\nu - \nu_0)/\Delta\nu_D$ , where  $\Delta\nu_D = v_{th}\nu_0/c$ , and  $v_{th}$  is the thermal velocity of the hydrogen atoms in the gas, given by  $v_{th} = \sqrt{2k_B T/m_p}$ , where  $k_B$  is the Boltzmann constant,  $T = 10^4$  K the gas temperature,  $m_p$  the proton mass and  $\nu_0 = 2.47 \times 10^{15}$  Hz is the Ly $\alpha$  resonance frequency. For reference, the optical depth through a column of hydrogen,  $N_{\text{HI}}$ , for a photon in the line center,  $\tau_0$ , is given by

$$\tau_0 = 5.9 \times 10^6 \left( \frac{N_{\text{HI}}}{10^{20} \text{ cm}^{-2}} \right) \left( \frac{T}{10^4 \text{ K}} \right)^{-0.5}. \quad (1)$$

The optical depth for a photon at a frequency  $x$  reduces to

$$\frac{\tau_x}{\tau_0} = \frac{a}{\pi} \int_{-\infty}^{\infty} \frac{e^{-y^2} dy}{(y-x)^2 + a^2} = \begin{cases} \sim e^{-x^2} & \text{core;} \\ \sim \frac{a}{\sqrt{\pi}x^2} & \text{wing,} \end{cases} \quad (2)$$

(e.g. Rybicki & Lightman 1979) where  $a$  is the Voigt parameter given by  $a = A_{21}/4\pi\Delta\nu_D = 4.7 \times 10^{-4} (v_{th}/13 \text{ km s}^{-1})^{-1}$ , where  $A_{21} = 6.25 \times 10^8 \text{ s}^{-1}$  is the Einstein A-coefficient for the transition. The transition between ‘wing’ and ‘core’ occurs at  $x \equiv x_t \approx 3.3$  for  $T = 10^4$  K.

Under most astrophysical conditions, absorption of a Ly $\alpha$  photon is followed by re-emission of a photon of the same energy in the frame of the atom. However, in the observer's frame the Ly $\alpha$  photon's energy before and after scattering is modified by Doppler shift due to the thermal motion of the atom, and scattering is only ‘partially’ coherent in the observer's frame. These Doppler shifts are important as they cause the photon's frequency to change by an *rms* shift of  $\Delta\nu_D$  per scattering event (Osterbrock 1962). Therefore, Ly $\alpha$  scattering through an optically thick medium can be described as a sequence of random walks in both frequency and real space (e.g. Harrington 1973; Neufeld 1990; Loeb & Rybicki 1999). Frequency diffusion is very efficient and spatial diffusion occurs predominantly when photons are in the wing of the line profile (e.g. Adams 1972; Harrington 1973). Hence, the last scattering event occurs in the wing of the line profile for the majority of Ly $\alpha$  photons emerging from an optically thick medium<sup>1</sup>.

Other quantities of relevance to our discussion are: (i) the scattering phase function (also known as the anisotropy function) which gives the probability  $p(\theta)$  that the scattered photon is re-emitted at an angle  $\theta$  relative to the incoming photon; and (ii) The degree of polarization  $\Pi(\theta)$  caused by scattering which is defined as  $\Pi(\theta) \equiv \frac{I_{||} - I_{\perp}}{I_{||} + I_{\perp}}$ , where  $I_{||}$  and  $I_{\perp}$  are the intensities parallel and perpendicular to the plane of scattering (defined by the wave vectors of the ingoing and outgoing photons), as a function scattering angle  $\theta$ . Both  $p(\theta)$  and  $\Pi(\theta)$  are different for core and wing scattering, as we discuss in more detail below.

### 2.2 Phase Function & Degree of Polarization for Ly $\alpha$ Scattering

For resonant scattering the phase function and the degree of polarization are strongly dependent on the atomic levels involved in the scattering event, and must be calculated quantum-mechanically. For example, the sequence of scattering events  $1S_{1/2} \rightarrow 2P_{1/2} \rightarrow 1S_{1/2}$  result in an unpolarized isotropically re-emitted Ly $\alpha$  photon, while the scattering events  $1S_{1/2} \rightarrow 2P_{3/2} \rightarrow 1S_{1/2}$  produce Ly $\alpha$  with a maximum polarization of  $\frac{3}{7}$  (e.g. Hamilton 1947; Chandrasekhar 1960; Ahn et al. 2002). Here we used a notation nL<sub>J</sub>, in which n, L and J are the principal quantum number, orbital angular momentum number, and total angular momentum number of the hydrogen atom involved in the scattering event, respectively. By summing over all possible Ly $\alpha$  transitions, the phase function and degree of

<sup>1</sup> Note that Ly $\alpha$  photons typically scatter only  $\sim \tau_0$  times before emerging from a medium of optical depth  $\tau_0$ , as opposed to the  $\tau_0^2$ -scaling, that is expected in the absence of frequency diffusion. For scattering events that occur in the wing, a so called ‘restoring force’ pushes the photon back towards the core by an average amount of  $-1/x$  (Osterbrock 1962; Adams 1972).

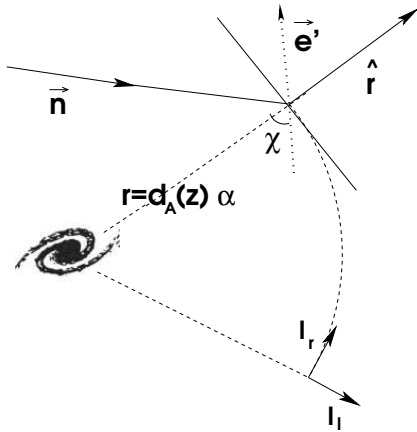


**Figure 1.** Schematic geometry of the last-scattering event of a Ly $\alpha$  photon that occurs at a radius vector  $\mathbf{r}$  away from the source galaxy. Before last scattering the photon's propagation direction is  $\mathbf{n}$  (which does not necessarily lie in the plane of the sky). After scattering, the photon travels in a direction  $\mathbf{n}'$  which is perpendicular to the sky plane. The polarization vector  $\mathbf{e}'$  after scattering lies in the plane of the sky and intersects the projected (on the sky plane) radius vector  $\mathbf{r}$  at an angle  $\chi$ . This photon contributes  $\cos^2 \chi$  and  $\sin^2 \chi$  to the intensity of the radiation field parallel ( $I_{\parallel}(\alpha)$ ) and perpendicular ( $I_{\perp}(\alpha)$ ) to  $\mathbf{r}$ , respectively. Here  $\alpha = r/d_A(z)$  (see text for additional details).

polarization for resonant scattering were found to be (e.g. Brandt & Chamberlain 1959; Bracken & Kyrola 1998)

$$p(\theta) = \frac{11}{12} + \frac{3}{12} \cos^2 \theta, \quad \Pi(\theta) = \frac{\sin^2 \theta}{\frac{11}{3} + \cos^2 \theta}. \quad (3)$$

As is shown in Appendix A, this corresponds to a case of a superposition of Rayleigh scattering plus isotropic scattering with corresponding weights of 1/3 and 2/3. The phase function  $p(\theta)$  satisfies  $\int p(\theta) d\Omega = 4\pi$ .

In quantum mechanics a Ly $\alpha$  scattering event cannot go separately through either  $1S_{1/2} \rightarrow 2P_{1/2} \rightarrow 1S_{1/2}$  or  $1S_{1/2} \rightarrow 2P_{3/2} \rightarrow 1S_{1/2}$ . Instead, each scattering event is a superposition of scattering through both levels simultaneously. Stenflo (1980) has shown that this introduces quantum interference terms which cause Ly $\alpha$  wing-scattering to be described by Rayleigh scattering for which

$$p(\theta) = \frac{3}{4} + \frac{3}{4} \cos^2 \theta, \quad \Pi(\theta) = \frac{\sin^2 \theta}{1 + \cos^2 \theta}. \quad (4)$$

This remarkable result implies that Ly $\alpha$  wing scattering can produce three times more polarization than Ly $\alpha$  resonant scattering (Stenflo 1980).

### 2.3 Incorporating Ly $\alpha$ Polarization in Radiative Transfer Codes

The code we used for the Monte-Carlo Ly $\alpha$  radiative transfer is described in Dijkstra et al. (2006). The code follows individual Ly $\alpha$  photons through spherical concentric shells with user-specified density and velocity fields. The code accurately describes the process of frequency and spatial diffusion in Ly $\alpha$  radiative transfer as described in § 2.1 (including other effects that were not discussed such as for example energy loss due to recoil). For a detailed description of the code, the interested reader is referred to Dijkstra et al.

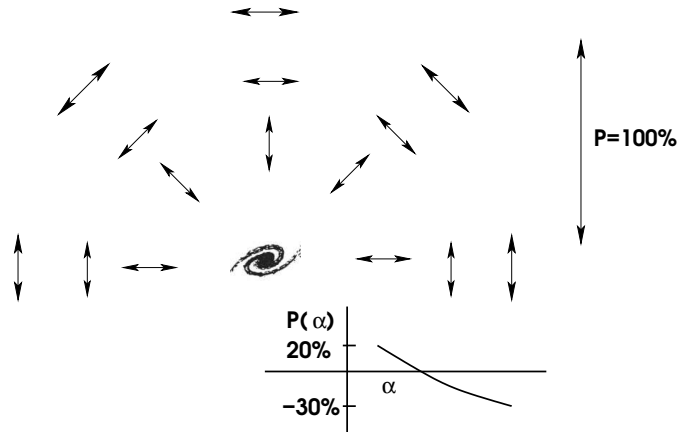


**Figure 2.** Schematic illustration of the polarization of scattered Ly $\alpha$  radiation. Arrows pointing away (towards) the galaxy represent a radiation field for which  $I_{\parallel} < I_{\perp}$  (i.e.  $\mathcal{P}(\alpha) > 0$ ), while  $I_{\parallel} > I_{\perp}$  is represented by arrows tangential to spheres of constant radius. The magnitude of the polarization is represented by the size of the arrows. The arrows vanish for unpolarized radiation. In all cases considered in this paper,  $\mathcal{P}(\alpha) < 0$  (this corresponds to a Stokes parameter  $Q < 0$ ), and the polarization vectors form concentric shells surrounding the central source.

(2006). The code was adapted to the context of this paper as follows:

- The modified code uses different phase functions for scattering in the core and wing as described in § 2.2. The original code (which was constructed for a different purpose) assumed only the Rayleigh scattering phase function.

- In § 2.2 we showed that the polarization of scattered Ly $\alpha$  photons depends strongly on whether Ly $\alpha$  was resonantly scattered or not. We also mentioned in § 2.1 that the transition between resonant and wing scattering occurs at  $x \sim 3.3$ . However, it is possible to determine whether a photon scattered resonantly for each scattering event directly from the Monte-Carlo simulation. While generating the velocity of the atom that scatters the Ly $\alpha$  photon, a scattering event is defined to be resonant if it occurred less than  $x_{\text{crit}} = 0.2$  Doppler widths away from resonance *in the frame of the atom involved in the scattering event* (see Appendix A for a justification of this number). The precise choice of  $x_{\text{crit}}$  does not affect our main results.

- The code was modified to include polarization based on the scheme developed by Rybicki & Loeb (1999). Although their method is applicable strictly to wing/Rayleigh scattering, only minor modifications are required to calculate polarization for resonantly scattered Ly $\alpha$  photons. This is mainly because resonant scattering is a superposition of isotropic and Rayleigh scattering. We will briefly discuss the Rybicki & Loeb (1999) method, before describing our modifications.

Rybicki & Loeb (1999) assigned 100% linear polarization to individual photons by endowing each Ly $\alpha$  photon with a polarization vector  $\mathbf{e}$ , which is perpendicular to the photon's propagation direction<sup>2</sup>  $\mathbf{n}$ , i.e.  $\mathbf{e} \cdot \mathbf{n} = 0$ . In this formulation, the Stokes parameters result from binning together multiple

<sup>2</sup> As mentioned in Rybicki & Loeb (1999), there is no need to consider circular polarization. Neither Rayleigh nor isotropic scat-

independent photons. The polarization vector after scattering ( $\mathbf{e}'$ ) is obtained by normalizing the vector  $\mathbf{g}'$ , which is obtained by projecting the polarization vector prior to scattering ( $\mathbf{e}$ ) onto the plane normal to the propagation direction ( $\mathbf{n}'$ ) of the photon after scattering. Symbolically,  $\mathbf{e}' = \mathbf{g}/|\mathbf{g}|$ , where  $\mathbf{g} = \mathbf{e} - (\mathbf{e} \cdot \mathbf{n}')\mathbf{n}'$ .

The observed radiation is characterized by its intensities parallel ( $I_l$ ) and perpendicular ( $I_r$ ) to the radius vector to the location of last scattering, denoted by  $\mathbf{r}$ , projected on the plane of the sky (see Figure 1), denoted by  $\hat{\mathbf{r}}$ . For the last scattering event  $\mathbf{n}'$  is perpendicular to the plane of the sky, and the polarization vector  $\mathbf{e}'$  lies in the plane of the sky (see Fig 1). We use  $\chi$  to denote the angle between the polarization vector  $\mathbf{e}'$  and  $\hat{\mathbf{r}}$ . A photon that is observed from impact parameter  $\alpha \equiv r/d_A(z)$  (with  $d_A(z)$  being the angular diameter distance to redshift  $z$ ) contributes  $\cos^2 \chi$  to  $I_l$  and  $\sin^2 \chi$  to  $I_r$  for Rayleigh (or wing) scattering (Rybicki & Loeb 1999).

However, for resonant scattering a photon contributes  $p_R \cos^2 \chi + \frac{1}{2}(1 - p_R)$  to  $I_l$  and  $p_R \sin^2 \chi + \frac{1}{2}(1 - p_R)$  to  $I_r$ . Here,  $p_R = (1 + \cos^2 \theta)/(11/3 + \cos^2 \theta)$  is the probability that a core photon was Rayleigh scattered in the last scattering event, in which  $\theta$  is the angle between the propagation directions of the incoming and outgoing photons at last scattering ( $\cos \theta = \mathbf{n} \cdot \mathbf{n}'$ ). The fact that  $p_R$  depends on angle  $\theta$  has a simple reason. Although resonant scattering may be viewed as a superposition of Rayleigh scattering and isotropic scattering of weights  $1/3$  and  $2/3$ , these weights are averaged over solid angle. The actual weight of each process is angle dependent (see Appendix A). In other words, in the case of resonant scattering the intensities in radial and azimuthal directions are obtained by scaling down the intensities obtained from Rayleigh scattering by a factor of  $p_R$ , and by adding an unpolarized intensity of magnitude  $1 - p_R$ .

The observed fractional polarization at impact parameter  $\alpha$  is given by

$$\mathcal{P}(\alpha) = \frac{|I_l(\alpha) - I_r(\alpha)|}{I_l(\alpha) + I_r(\alpha)}. \quad (5)$$

The fractional polarization can also be expressed in terms of the Stokes parameters  $Q$  and  $I$  as  $\mathcal{P} = |Q|/I$ . In this paper, we always find that  $I_l < I_r$ , and  $Q < 0$ . This may be represented by arrows drawn in concentric rings around the central Ly $\alpha$  emitter, where the size of an arrow indicates the magnitude of  $\mathcal{P}$  (see Fig 2).

- Monte-Carlo calculations of Ly $\alpha$  transfer can be accelerated by skipping scattering events that occur in the line core (e.g. Ahn et al. 2002; Dijkstra et al. 2006). One has to be careful when applying this technique in calculations of polarization, as it reduces the number of scattering events that a Ly $\alpha$  photon encounters and hence distorts its resulting polarization state. For this reason, we have not sped up the calculations with this technique.

Lastly, we point out that the expressions for  $p(\theta)$  and  $\Pi(\theta)$  in § 2.2 were derived under the assumption that the radiation field prior to the scattering event was unpolarized. The precise functional forms of  $p(\theta)$  and  $\Pi(\theta)$  are different when the radiation field prior to scattering is polarized

tering can generate circular polarization, except from circularly polarized light.

(see Appendix A). To account for the precise polarization dependence of  $p(\theta)$  and  $\Pi(\theta)$  one must use the density matrix formalism (e.g. Lee 1994; Lee & Ahn 1998; Ahn et al. 2002). However, the procedure of propagating the polarization vector in a single scattering event that was outlined above, naturally accounts for the polarization dependence of  $\Pi(\theta)$ . Rybicki & Loeb (1999) successfully tested their procedure (i) against analytic calculations performed by Schuster (1879), and (ii) by solving the Milne problem for a Rayleigh scattering atmosphere. The precise dependence of  $p(\theta)$  on the polarization of the incoming radiation is therefore not important. The dependence of  $p(\theta)$  and  $\Pi(\theta)$  on initial polarization does not affect the calculations regarding resonant scattering either. The maximum fractional polarization we find for resonantly scattered Ly $\alpha$  is 7% (see § 3.2). The typical polarization of the Ly $\alpha$  radiation field ‘seen’ by atoms involved in the scattering process is even lower. This only introduces changes in the phase function at the level of a few per cent, and we have verified that our results regarding resonantly scattered Ly $\alpha$  are insensitive to the precise form of the phase function.

### 3 LY $\alpha$ POLARIZATION AROUND HIGH-REDSHIFT SOURCES

Next we calculate the expected polarization of the Ly $\alpha$  line in a set of models which span the likely environments of high-redshift galaxies. Unless otherwise stated, we assume the redshift of Ly $\alpha$  sources to be  $z = 5.7$  in all cases. The Monte-Carlo radiative transfer calculations rely on stacking individual photons into bins, and the errorbars shown in some figures were calculated assuming Poisson fluctuations in the number of photons within a given bin.

#### 3.1 Backscattering off Galactic Superwinds

##### 3.1.1 Description of the Model

A major fraction of Lyman break galaxies (LBGs) at high redshifts show evidence of being surrounded by outflowing enriched gas (Shapley et al. 2003). Scattering of Ly $\alpha$  photons by neutral hydrogen atoms in these outflows may cause the observed Ly $\alpha$  line to be redshifted systematically relative to the systemic velocity of the galaxy (Ahn et al. 2003). This redshift is attributed to the Doppler boost that Ly $\alpha$  photons experience when they scatter off the outflow on the far side of the galaxy back towards the observer (hence the term ‘backscattering’). This redshifted Ly $\alpha$  flux is less prone to resonant scattering in the IGM, and is therefore more easily observable than Ly $\alpha$  photons that were not backscattered.

The impact of the outflow of the observable properties of the Ly $\alpha$  line depends on various parameters including the outflow speed,  $v_{\text{exp}}$ , the total column density of neutral hydrogen atoms in the outflow,  $N_{\text{HI}}$ , and the dust content and distribution inside the outflow (Hansen & Oh 2006; Verhamme et al. 2006). We show results for  $N_{\text{HI}} = 10^{19} \text{ cm}^{-2}$  and  $N_{\text{HI}} = 10^{20} \text{ cm}^{-2}$ , based on column densities that are observed in Ly $\alpha$  emitting galaxies (Kunth et al. 1998; Verhamme et al. 2008). We discuss the choice of our model in more detail after presenting our results below. The outflow speed is typically of order the circular velocity of the

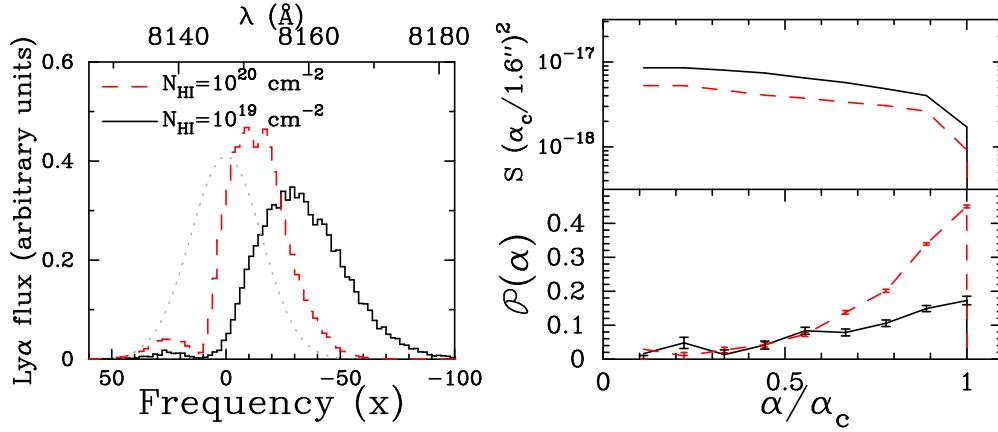


**Figure 3.** The observable properties of the Ly $\alpha$  radiation emitted by a galaxy which is surrounded by a spherical shell of gas that expands at a speed  $v_{\text{exp}} = 200 \text{ km s}^{-1}$  and contains neutral hydrogen with a column density of either  $N_{\text{HI}} = 10^{19} \text{ cm}^{-2}$  (red dashed lines) or  $N_{\text{HI}} = 10^{20} \text{ cm}^{-2}$  (solid lines). These parameter choices represent the generic conditions in galaxies surrounded by a superwind driven outflow (see text). The dotted line in the left panel shows the Gaussian Ly $\alpha$  emission line prior to scattering. The figure shows that backscattering off the expanding outflow results in a systematic redshift of the Ly $\alpha$  line. The top and bottom right panels show the surface brightness profile (units are  $\text{erg s}^{-1} \text{ cm}^{-2} \text{ arcsec}^{-2}$ ) and fractional polarization  $\mathcal{P}(\alpha)$  as a function of  $\alpha$ , respectively. Here, the amplitude of  $\alpha$  and the surface brightness  $S(\alpha)$  are written in terms of  $\alpha_c$ , which is related to the distance of the expanding shell from the galaxy (see text). The Figure shows that the polarization reaches values as high as  $\sim 40\%$ .

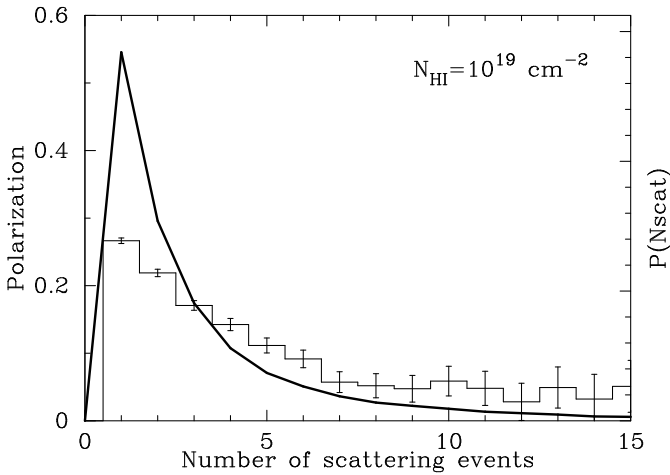


**Figure 4.** The histogram shows the angle-averaged polarization as a function of the number of times Ly $\alpha$  photons scatter for the superwind model with  $N_{\text{HI}} = 10^{19} \text{ cm}^{-2}$ . The angle-averaged polarization is largest for photons that scatter only once ( $\langle \mathcal{P}(\alpha) \rangle \sim 30\%$ ), and almost vanishes for  $N_{\text{scat}} \geq 10$ . The thick solid line shows the probability distribution of the number of times Ly $\alpha$  photons scatter. Clearly, the majority of photons scatter only once, which causes the observed Ly $\alpha$  flux to be highly polarized.

host dark matter halo,  $v_{\text{circ}}$  (e.g. Furlanetto & Loeb 2003). We assume the galaxy to be embedded in a halo of total mass  $M_{\text{tot}} = 3 \times 10^{11} M_{\odot}$ , which corresponds to  $v_{\text{circ}} = 200 \text{ km s}^{-1}$ .

### 3.1.2 Results

The emitted Ly $\alpha$  spectrum prior to scattering is assumed to be a Gaussian with a velocity width  $\sigma = v_{\text{circ}}$  (Dijkstra et al 2007) and is denoted by the dotted line in the left panel of Figure 3. The dashed (solid) lines represent the

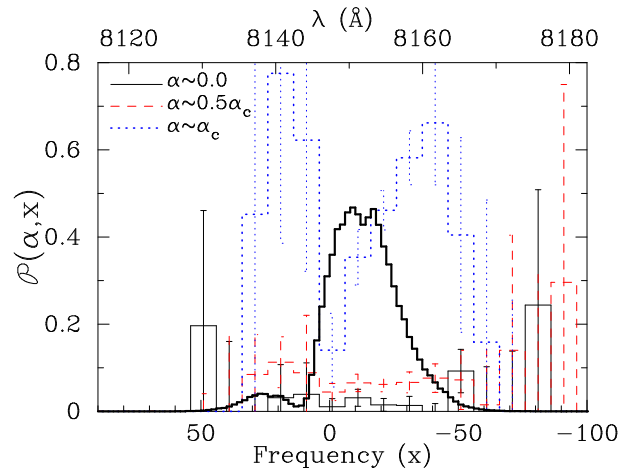


**Figure 5.** The frequency dependence of the polarization at  $\alpha = 0$  (thin black histogram),  $0.5\alpha_c$  (red dashed histogram), and  $\alpha_c$  (blue dotted histogram). The polarization increases with impact parameter. The thick solid line shows the observed spectrum which was also shown in Fig 3 (the units are arbitrary). The bulk of the photons have frequencies  $-50 < x < 10$ . Within this frequency range, the polarization increases towards the red. This is because the redder Ly $\alpha$  photons appear farther from resonance in the frame of the expanding gas; consequently they scatter less and achieve a higher polarization amplitude (see Fig 4). This generic frequency dependence of the polarization amplitude can be used as a fingerprint of outflows. The frequency dependence is reversed for infalling gas (see § 3.3).

observed spectrum for an outflow with  $N_{\text{HI}} = 10^{19} \text{ cm}^{-2}$  ( $10^{20} \text{ cm}^{-2}$ ). The Figure shows that backscattering off the expanding outflow results in a systematic redshift of the Ly $\alpha$  line (as mentioned above), with an increase in redshift as  $N_{\text{HI}}$  increases. The top right panel shows that the surface brightness profile remains flat out to some value of  $\alpha = \alpha_c$  after which it drops to zero (as there is no scattering outside the shell). The magnitude of  $\alpha_c$  and the surface

brightness  $S(\alpha) \equiv I_1(\alpha) + I_r(\alpha)$  are determined by the radius of the expanding shell. For example, if the outflow is located at a distance  $d = 10$  kpc from the central galaxy (and its thickness  $\ll d$ ), then the surface brightness profile drops to zero at  $\alpha_c = 1.6''(d/10 \text{ kpc})$  for a galaxy at  $z = 5.7$ . The mean surface brightness scales approximately as  $S(\alpha) \approx \mathcal{X} \times 10^{-18} (\alpha_c/1.6'')^{-2} (L_{\text{Ly}\alpha}/10^{43} \text{ erg s}^{-1}) \text{ erg s}^{-1} \text{ cm}^{-2} \text{ arcsec}^{-2}$ , where  $\mathcal{X} = 3$  for  $N_{\text{HI}} = 10^{19} \text{ cm}^{-2}$ , and  $\mathcal{X} = 5$  for  $N_{\text{HI}} = 10^{20} \text{ cm}^{-2}$ .

The *bottom right panel* shows that the fractional polarization,  $\mathcal{P}(\alpha)$ , increases towards larger values of  $\alpha$  and reaches a maximum near  $\alpha_c$ . The polarization amplitude obtains values as high as  $\sim 40\%$  for  $N_{\text{HI}} = 10^{19} \text{ cm}^{-2}$ , and  $\sim 18\%$  for  $N_{\text{HI}} = 10^{20} \text{ cm}^{-2}$ .

The reason for the overall large values of the polarization is easy to understand. Although the line center optical depth through the outflow is very large for both models,  $\tau_0 = 5.9 \times 10^5 (N_{\text{HI}}/10^{19} \text{ cm}^{-2})$  (see Eq 1), most photons reside in the wings of the line profile when they reach the expanding shell. For example, in the model with  $N_{\text{HI}} = 10^{19} \text{ cm}^{-2}$ , the optical depth is less than unity for 63% of the photons when they enter the outflow for the first time. Therefore, most photons scatter only once in the wing of the line profile before escaping to the observer.

The above interpretation is quantified by Figure 4, in which the *thick solid line* shows the probability distribution for the number of scattering events encountered by the Ly $\alpha$  photons,  $P(N_{\text{scat}})$ . The function  $P(N_{\text{scat}})$  peaks at  $N_{\text{scat}} = 1$  and rapidly decreases for increasing  $N_{\text{scat}}$ . Also shown as the *histogram* is the angle-averaged polarization of the photons as a function of  $N_{\text{scat}}$ . The polarization is largest for photons that scatter only once ( $\langle P(\alpha) \rangle \sim 30\%$ ), and nearly vanishes for  $N_{\text{scat}} \geq 10$ . The decrease in the polarization amplitude with increasing  $N_{\text{scat}}$  reflects that the radiation field becomes increasingly isotropic as the number of scattering events increases. As  $N_{\text{HI}}$  increases, the fraction of photons that escape after a single scatter decreases, and the overall polarization declines.

Figure 5 shows the frequency dependence of the polarization at three different impact parameters, namely  $\alpha = 0$  (*thin black histogram*),  $0.5\alpha_c$  (*red dashed histogram*), and  $\alpha_c$  (*blue dotted histogram*). As already illustrated in Figure 3, the polarization increases with increasing impact parameter. The *thick solid line* shows the observed spectrum which was previously shown in Fig 3. The bulk of photons have frequencies  $-50 < x < 10$ . Within this frequency range, the polarization increases towards the red. This is because the redder Ly $\alpha$  photons appear farther from resonance in the frame of the gas; they therefore scatter less and achieve a higher polarization amplitude (see Fig 4). This frequency dependence of the polarization can be used as a fingerprint to distinguish outflows from infall (see § 3.3). Interestingly, the polarization observed from impact parameter  $\alpha \sim \alpha_c$  goes through a minimum at  $x \sim 0$  (*blue dotted histogram*). This feature originates from the fact that the photons observed at this frequency were at resonance in the frame of the outflowing gas; this in turn increases the number of times these photons scattered which in turn decreases their net level of polarization.

One may wonder whether the above results depend sensitively on the assumed model: e.g. do the result change for a continuous, dusty, wind with a radial dependence of

its outflow speed? A wind for which the outflow speed increases linearly with radius would resemble the IGM with a Hubble flow as discussed in Rybicki & Loeb (1999), who found even higher levels of polarization. Furthermore, scattering through an optically thick *collapsing* gas cloud also results in a comparable polarization ( $\mathcal{P}_{\text{max}} \sim 35\%$ , see § 3.3). Changing the sign of the velocity of the gas only affects the frequency dependence of the polarization (see § 3.3). The column density of neutral hydrogen in both these models is  $N_{\text{HI}} \gg 10^{20} \text{ cm}^{-2}$ , which implies that polarized Ly $\alpha$  is also expected for outflow models with larger column densities and non-zero velocity gradients.

Furthermore, the presence of dust in the expanding wind can boost the polarization. The reason is that photons that scatter only once obtain the highest level of polarization, while it decreases for photons that scatter multiple times (Fig 4). However, photons that scatter multiple times traverse a longer path through the wind, which enhances the probability for absorption by dust. Hence, dust can preferentially quench the low polarization photons, which would strengthen our results.

## 3.2 Resonant Scattering in the IGM

### 3.2.1 Description of the Model

Even after reionization, residual neutral hydrogen in the IGM can scatter up to  $\gtrsim 90\%$  of the Ly $\alpha$  emitted by galaxies out of our line of sight (Santos 2004; Dijkstra et al. 2007b). This scattered Ly $\alpha$  radiation would appear as a faint Ly $\alpha$  halo surrounding the central Ly $\alpha$  emitting galaxy (Loeb & Rybicki 1999). We note that back-scattered Ly $\alpha$  radiation is much less prone to resonant scattering in the IGM. Therefore we now consider galaxies that are not surrounded by wind-driven outflows, and examine examples that complement the cases discussed previously.

We adopt the fiducial model described by Dijkstra et al. (2007b) to examine the impact of the IGM on the observed Ly $\alpha$  line profile of a  $z = 5.7$  galaxy embedded in a dark matter halo with a total mass of  $M_{\text{tot}} = 10^{11} M_{\odot}$ . The halo has a virial radius  $r_{\text{vir}} = 23$  kpc and a circular velocity  $v_{\text{circ}} = 133 \text{ km s}^{-1}$ . The galaxy is assumed to form stars at a rate of  $\dot{M}_{\star} = 10 M_{\odot} \text{ yr}^{-1}$ , and the escape fraction of its ionizing photons is taken to be  $f_{\text{esc}} = 0.1$ . The resulting Ly $\alpha$  luminosity of the galaxy is  $L_{\text{Ly}\alpha} = 2 \times 10^{43} \text{ erg s}^{-1}$  for a gas metallicity of  $Z = 0.05 Z_{\odot}$  (see Dijkstra et al 2007 for a more detailed description and a motivation of this model). The observable properties of the Ly $\alpha$  photons that were resonantly scattered in the IGM are shown<sup>3</sup> in Figure 6.

We also examine a case where we artificially boost the photoionization rate in the IGM. This boost may represent:

<sup>3</sup> Dijkstra et al. (2007b) account for gas clumping in the IGM. Most of the volume of the IGM consists of interclump gas that is underdense. For this reason the mean IGM opacity to Ly $\alpha$  photons is lower in a clumpy IGM at a fixed value of the ionizing background (Dijkstra et al 2007). Because clumps are not included in the radiative transfer code, we increased the ionizing background (compared to the clumpy case) in order to match the observed mean transmission of the IGM at a redshift  $z$ ,  $\langle e^{-\tau} \rangle(z)$  (e.g. Fan et al. 2006).

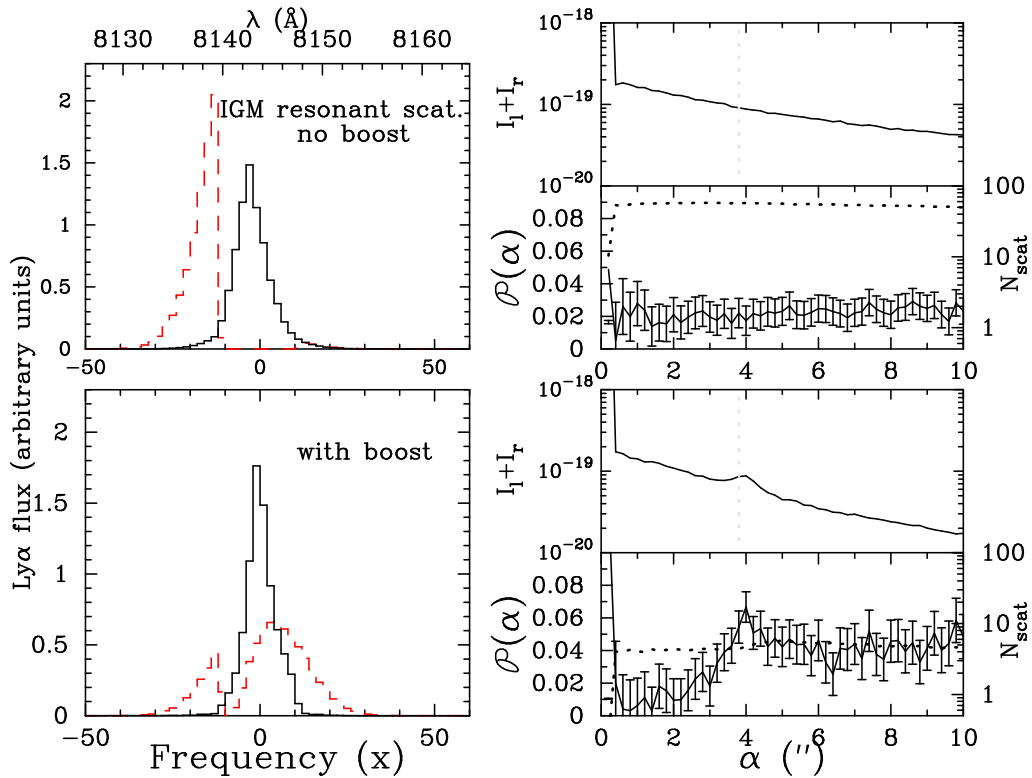


**Figure 6.** The observable properties of Ly $\alpha$  radiation that is resonantly scattered in the intergalactic medium (IGM). The cases considered here represent galaxies that are not surrounded by a superwind-driven outflow and complement the examples shown in Fig 3 (see text). The IGM is assumed to have a peculiar infall velocity (see text). The *upper left panel* shows the spectrum of unscattered Ly $\alpha$  as the *red dashed line*, and the spectrum of the resonantly scattered Ly $\alpha$  as the *solid line* (both spectra are normalized). The unscattered spectrum reflects the line-emission spectrum observed from the galaxy (see text). The *upper right panels* show that the fractional polarization is only  $\mathcal{P}(\alpha) \sim 2\%$ . The main reason is that each photon resonantly scatters  $\sim 50$  times, as shown by the *dotted line*. The *lower panels* show the results for the same calculation but with an increased level of the ionizing background. The boost in the ionizing background increases the transmission on the blue-side of the line (*lower left panel*). In this case each Ly $\alpha$  photon scatters on average only a few times, and the scattered Ly $\alpha$  is polarized up to  $\sim 7\%$  (*lower right panels*). Thus, the polarization of resonantly scattered Ly $\alpha$  photons in the IGM is low compared to that in § 3.1, and its level depends on the local level of the ionizing background.

(i) an enhanced local ionizing background due to clustering of undetected surrounded sources (Wyithe & Loeb 2005; Dijkstra et al. 2007b); (ii) an enhanced ionizing background due to the presence of a nearby quasar; (iii) a galaxy at a lower redshift where the residual neutral hydrogen fraction in the IGM is lower; (iv) an enhanced local photoionization rate due to vigorous star formation in the galaxy itself, or due to an enhanced escape fraction of ionizing photons; (v) a lower neutral fraction because of a lower overall density of hydrogen nuclei along the line of sight (e.g. for a galaxy on the edge of a void.)

### 3.2.2 Results

In the *top left panel* of Figure 6 we show the spectrum of unscattered Ly $\alpha$  radiation (*dashed line*), which shows the line-emission spectrum observed from the galaxy. The spectrum of the resonantly scattered Ly $\alpha$  halo is shown as the *solid line*. The unscattered spectrum was the focus of the analysis of e.g. Santos (2004) and Dijkstra et al. (2007b). The plot shows that the blue side of the Ly $\alpha$  line observed from the galaxy ( $x > 0$ ) is eliminated by the IGM. The suppression extends into the red part of the line because of resonant scattering by residual neutral hydrogen gas that is falling onto

the galaxy. Therefore, the peak of the observed spectrum is redshifted relative to the true line center by an amount which is set by the gas infall velocity. The redshift in velocity is  $v_{\text{IGM}}(r_{\text{vir}}) = -v_{\text{circ}}$ .

The *top right panel* of Figure 6 shows the surface brightness profile of the scattered Ly $\alpha$  halo as a function of  $\alpha$ . The observed surface brightness of the scattered Ly $\alpha$  photons is  $\sim 10^{-19} \text{ erg s}^{-1} \text{ cm}^{-2} \text{ arcsec}^{-2}$  near the center, and decreases with increasing angular separation from the galaxy. Overall, the fractional polarization is small,  $\mathcal{P}(\alpha) \sim 2\%$ . Besides the fact that resonantly scattered Ly $\alpha$  radiation is always less polarized than the radiation in the line wings (see § 2.2), there is the fact that when the Ly $\alpha$  enters resonance, it typically scatters multiple times before escaping towards the observer. This is shown by the *dotted line* which gives the mean number of scattering events for the Ly $\alpha$  photons,  $\langle N_{\text{scat}} \rangle$ , as a function of impact parameter  $\alpha$ . In this model  $\langle N_{\text{scat}} \rangle \sim 50$ . Hence, the Ly $\alpha$  radiation field of resonantly scattered Ly $\alpha$  photons will locally be close to isotropic, resulting in a low polarization.

The *lower panels* in Figure 6 show the results for the model in which the ionizing background was boosted. The *lower left panel* shows that boosting the photoionization rate decreases the fraction of residual neutral hydrogen gas,

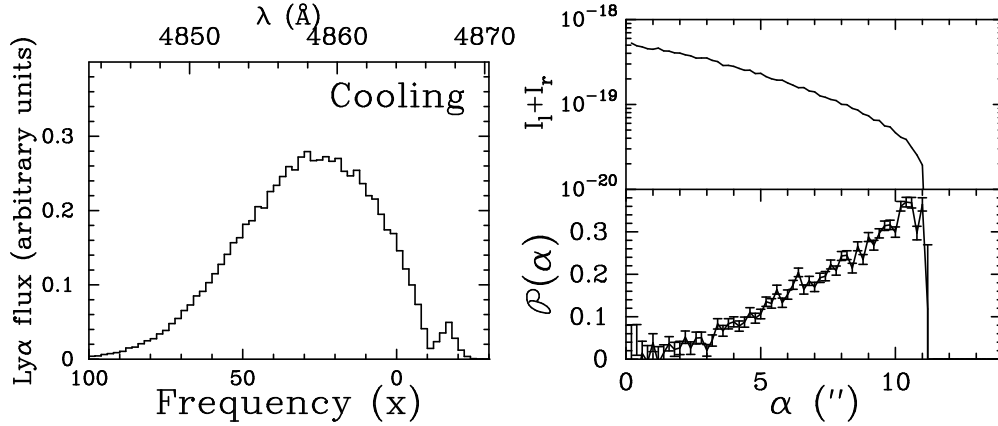


**Figure 7.** The observable properties of Ly $\alpha$  radiation emerging from a neutral collapsing gas cloud. The model represents protogalaxies in the process of their assembly. The *left panel* shows that the spectrum emerging from such a cloud has a systematic blueshift. The *right panel* shows that the Ly $\alpha$  surface brightness profile (units are  $\text{erg s}^{-1} \text{cm}^{-2} \text{arcsec}^{-2}$ ) is rather flat (*top*), and that it is highly polarized. The fractional polarization increases roughly linearly towards the edge of the cloud, and reaches a maximum value of  $\mathcal{P}_{\text{max}} \sim 35\%$ .

which in turn increases the transmission on the blue-side of the line. The *lower right panels* show that the surface brightness profile falls slightly faster with a slight peak in the surface brightness profile near the virial radius. The reason for this peak is that in our model the IGM is densest right outside the virial radius, which results in the largest effective optical depth here (this also produces the dip in the spectrum). In this model each Ly $\alpha$  photon scatters on average only a few times which causes the scattered Ly $\alpha$  to be polarized up to  $\sim 7\%$ .

In summary, the polarization of resonantly scattered Ly $\alpha$  photons in the IGM is low compared to the values derived in § 3.1, with the maximum polarization level reaching values of  $\mathcal{P}_{\text{max}} \lesssim 7\%$ . The polarization amplitude depends strongly on the local level of the ionizing background. This is because the polarization decreases with increasing effective optical depth,  $\tau_{\text{eff}}$ , which in turn increases with a decreasing local photoionization rate.

### 3.3 Scattering in Optically Thick Clouds

#### 3.3.1 Description of the Model

Dijkstra et al. (2006) performed Monte-Carlo calculations of Ly $\alpha$  radiative transfer through optically thick, spherically symmetric, collapsing gas clouds, which represent simplified models of protogalaxies in the process of their assembly. Here we compute the Ly $\alpha$  polarization properties for one of the fiducial models presented by Dijkstra et al. (2006), in which a dark matter halo of mass  $M_{\text{tot}} = 5.2 \times 10^{11} M_{\odot}$  collapses at  $z = 3$  while it continuously emits Ly $\alpha$  over a spatially extended region (see ‘model 1.’ of Dijkstra et al 2006).

#### 3.3.2 Results

The *left panel* of Figure 7 shows that the Ly $\alpha$  emerges with a systematic blueshift, which is due to energy transfer from the gas to the photons, combined with a reduced escape probability for photons in the red wing of the line profile (see Dijkstra et al. 2006, for a detailed discussion). The spectrum looks noisier than that shown in Dijkstra et al (2006)

due to the small number of photons ( $\sim 10^4$ ) used in the Monte-Carlo calculation here (in which the code was not artificially accelerated), but otherwise identical. The *right panels* of Figure 7 show the surface brightness profile (*top*), and the fractional polarization  $\mathcal{P}(\alpha)$  (*bottom*) as a function of  $\alpha$ . The fractional polarization again reaches values as high as  $\mathcal{P}_{\text{max}} = 35\%$ . This may be surprising given the fact that each photon scatters numerous times before emerging from the cloud. As mentioned in § 2.1, Ly $\alpha$  photons generally escape from an optically thick medium in the line wing, where they acquire larger polarizations than in the line core. Furthermore, each spherical shell inside the cloud must see a net outward flow of Ly $\alpha$  photons, or else the cloud would not cool. Therefore, the radiation field appears anisotropic to atoms inside the cloud at all radii and observed photons that were scattered inside the cloud must have a net polarization. The magnitude of the polarization is a measure of the anisotropy of the radiation field.

In Figure 8 we show the frequency dependence of the polarization at 3 different angular separations:  $\alpha \sim 0, 5.5$ , and 10 arcseconds. The *thick solid line* is the spectrum shown previously in Figure 7, indicating that the bulk of the photons emerge with frequencies  $-10 < x < 80$ . Within this frequency range, the polarization increases towards the blue (although this trend is less obvious than in § 3.1). The reason for this wavelength dependent polarization is that Ly $\alpha$  photons that are far in the blue wing of the line profile, appear even farther in the wing in the frame of the infalling gas. Therefore, the escape probability of Ly $\alpha$  photons increases, and the radiation field becomes increasingly anisotropic towards higher photon frequencies. This in turn increases the polarization towards higher frequencies.

## 4 DISCUSSION

### 4.1 Constraints on EoR and High- $z$ Galaxy Formation

The Ly $\alpha$  emission needs to be spatially resolved in order for its polarization to be measured. Over the past decade, a large number of spatially extended Ly $\alpha$  emitters, also



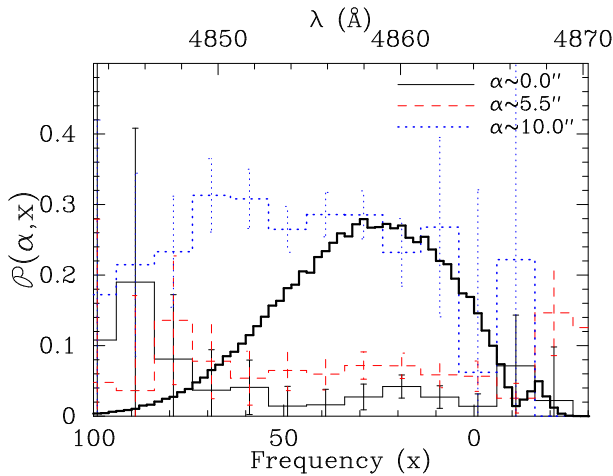


**Figure 8.** The frequency dependence of the polarization at three different angular separations from the galaxy:  $\alpha \sim 0, 5.5$ , and  $10$  arcseconds. The polarization increases with separation (as was already demonstrated in Fig 7). The thick solid line shows the spectrum (arbitrary units, previously shown in Figure 7). The bulk of the photons emerge with frequencies  $-10 < x < 80$ . Within this frequency range, the polarization increases mildly towards higher frequencies, in sharp contrast with the outflow model discussed in § 3.1.

known as Ly $\alpha$  ‘blobs’, were discovered (Steidel et al. 2000; Matsuda et al. 2004; Saito et al. 2006). In fact, the size distribution of Ly $\alpha$  sources is continuous and Ly $\alpha$  blobs simply represent the largest and rarest objects in this distribution (Matsuda et al. 2004). This implies that there is no shortage of spatially extended Ly $\alpha$  sources in the Universe.

As was shown in § 3, the polarization properties of spatially resolved Ly $\alpha$  emission encode information about the medium through which the Ly $\alpha$  photons propagate, especially in combination with spectral information (Fig 5 and Fig 8). For example, large fractional polarizations (tens of percent) are expected for Rayleigh scattering. An increase in the polarization towards longer wavelengths would be indicative of backscattering off an expanding outflow. Such an inference could be particularly important because (i) it provides evidence that the extended Ly $\alpha$  emission results from scattering (ii) it allows to better gauge the impact of resonant scattering in the IGM on the observed Ly $\alpha$  line profile, since back-scattered Ly $\alpha$  radiation is much less prone to resonant scattering in the IGM. Understanding the impact of resonant scattering on the Ly $\alpha$  line profiles is essential for (iii) deriving constraints on the ionization state of the IGM (Dijkstra et al. 2007a), and (iib) interpreting Ly $\alpha$  emitters with large equivalent widths (Malhotra & Rhoads 2002; Dijkstra & Wyithe 2007).

In this paper we have shown numerical examples for the polarization properties of Ly $\alpha$  radiation that is either (i) resonantly scattered in the IGM; (ii) backscattered in an outflow; or (iii) associated with cooling radiation from a collapsing protogalaxy. There are other classes of spatially extended Ly $\alpha$  sources that have not been discussed:

- Gas in close proximity to a bright source of ionizing radiation (e.g. a quasar) may ‘glow’ in fluorescent Ly $\alpha$  emission (Haiman & Rees 2001; Weidinger et al. 2004). If the recombining Ly $\alpha$  emitting gas is sufficiently close to the quasar

or the quasar is particularly bright, then this gas is optically thin to Ly $\alpha$  photons and the emergent Ly $\alpha$  radiation is not expected to be polarized. However, fluorescent Ly $\alpha$  emission is also expected from Lyman limit systems and Damped Ly $\alpha$  systems (Gould & Weinberg 1996; Cantalupo et al. 2005; Adelberger et al. 2006; Cantalupo et al. 2007), which are optically thick to Ly $\alpha$ . Especially in cases where the gas is illuminated anisotropically, scattering could lead to a detectable polarization.

- Spatially extended Ly $\alpha$  emission may be generated by gas that was shock heated by a superwind-driven outflow (e.g. Taniguchi & Shioya 2000; Mori et al. 2004). The backscattering mechanism described in § 3.1 may also operate here, and this could lead to a measurable polarization amplitude.

- Extended luminous Ly $\alpha$  emission is common around radio galaxies, and is thought to be powered by a jet-IGM interaction (e.g. Chambers et al. 1990). Little is known about the source of the Ly $\alpha$  emission and to what degree the Ly $\alpha$  is scattered by residual neutral gas. Polarimetry may provide new insights on the nature of these sources.

We have focused on spatially extended Ly $\alpha$  sources, as the polarization averages out to zero for a symmetric unresolved source. However, as was shown by Lee & Ahn (1998), anisotropic outflows (e.g. biconical outflows) may still result in observable polarization, even if the Ly $\alpha$  source is completely unresolved. Hence, a measurable polarization may not be restricted to spatially resolved Ly $\alpha$  sources.

Lastly, we point out that accurate polarization measurements of faint high-redshift sources is difficult. It would therefore be prudent to obtain polarimetry of the brightest sources first. This approach will likely lead to insights about the processes that regulate the transfer of Ly $\alpha$  in and around high-redshift galaxies.

## 4.2 Comparison to Polarization of Foregrounds

The dominant foregrounds in the infrared sky (at wavelengths  $\lambda < 2\mu\text{m}$ ), are Rayleigh scattered moonlight and starlight (e.g. Glass 1999, p.33), and are therefore polarized. However, line emitters can easily be extracted from this scattered foreground for which the spectrum is continuous. Here, we investigate whether Ly $\alpha$  emitters can be distinguished from foreground line emitters, such as [OII], [OIII], H $\alpha$ , and H $\beta$  emitters, based on their polarization properties.

In practice it has been possible to effectively discriminate between these low-redshift interlopers and actual high-redshift Ly $\alpha$  emitters based on broad-band colors and on the shape of the Ly $\alpha$  line (e.g. Kashikawa et al. 2006). However, the continuum spectrum of some Ly $\alpha$  emitters with a large equivalent width is difficult to detect, and in some cases the Ly $\alpha$  line is not asymmetric (see e.g. the lower left panel of Fig 6).

The possibility that high-redshift Ly $\alpha$  emitters are highly polarized may provide another diagnostic that distinguishes them from low-redshift interlopers. A low level of polarization ( $P \lesssim 2\%$ ) is expected for any extragalactic line emitter due to scattering by dust in the Milky-Way (Schmidt & Miller 1985). Furthermore, spatially resolved [OIII] line emission at higher levels of polarization ( $P \sim 4\%$ ) has been observed in a small fraction of Seyfert

2 galaxies (Goodrich 1992). This polarization arises when the narrow line region is obscured. In this case, the only [OIII] photons that are observed are scattered towards the observer, either by dust or by electrons. This same mechanism could produce polarized [OII], H $\alpha$  and H $\beta$  line emission. This suggests it is risky to distinguish high-redshift Ly $\alpha$  emitters from low-redshift interlopers on the basis of polarimetry. On the other hand, the observed levels of polarization in low-redshift interlopers are small compared to the values we find in our models, which suggests that high levels of polarization ( $\mathcal{P} \sim 10\%$ ) are indicative of scattered Ly $\alpha$ .

Raman scattering of Ly $\beta$  wing photons may produce highly polarized H $\alpha$  emission in a radiative cascade of the form  $3p \xrightarrow{H\alpha} 2s \xrightarrow{2\gamma} 1s$  (e.g. Lee & Yun 1998; Yoo et al. 2002). This mechanism requires the presence of large HI column densities  $N_{\text{HI}} \gtrsim 10^{20} \text{ cm}^{-2}$ , and has been observed to operate around symbiotic stars (Ikeda et al. 2004), and potentially in close proximity to quasars (Lee & Yun 1998). In distant galaxies, however, these emission regions would be completely unresolved, and the polarization averages out to zero. On the other hand, columns in excess of  $N_{\text{HI}} \gtrsim 10^{20} \text{ cm}^{-2}$  can easily exist in the neighborhood of galaxies, and it is not possible to rule out altogether the possibility of highly polarized H $\alpha$  emission as a contaminant of polarized Ly $\alpha$  emitters. Nevertheless, polarized H $\alpha$  lines produced by this mechanism are typically broad (FWHM  $\sim 20 - 40 \text{ \AA}$ ) and symmetric, with wings extending into both the longer and shorter wavelengths (see e.g. Yoo et al. 2002, their Fig 4-8); these features clearly distinguish them from Ly $\alpha$  line emitters.

Ground-based searches for high-redshift Ly $\alpha$  emitters are complicated by the presence of bright OH emission lines, which are produced by the excited radical OH\* in the ionosphere, following the reaction  $\text{H} + \text{O}_3 \rightarrow \text{OH}^* + \text{O}_2$  (e.g. Glass 1999). These lines make up the Meinel bands (Meinel 1950a,b) and are typically much brighter than Ly $\alpha$  sources. Furthermore, these lines exhibit large temporal and spatial variations in intensity due to the passage of density waves through the ionosphere (Ramsay et al. 1992). However, the wavelengths of these lines are well known, and future instruments (such as e.g. the Dark Age Z Ly $\alpha$  Explorer, Horton et al. 2004) intend to search for redshifted ( $z = 6.5 - 12$ ) Ly $\alpha$  lines between these lines using high-resolution ( $R = 1000$ ) spectrographs.

Polarimetry may provide an interesting alternative method of suppressing OH-emission lines. Although the OH-lines have been studied in detail (e.g. Ramsay et al. 1992; Maihara et al. 1993), we are unaware of any polarization measurements. If OH-lines are unpolarized, then polarimetry may be used to remove them efficiently<sup>4</sup>. For example,

<sup>4</sup> The Meinel bands correspond to rotational and vibrational states of the OH-molecule. It is conceivable that the earth's magnetic field introduces a preferred axis of rotation and/or vibration, which would induce some level of polarization to the lines. However, any large-scale polarization of the foreground OH lines due to the Earth's magnetic field would not have structure on the scales of tens of arcseconds and would therefore be distinguishable from the arc-like features of scattered Ly $\alpha$  radiation around high-redshift galaxies. After removing any uniform polarization component, the remaining foreground should be unpolarized on

consider an unpolarized OH sky line that is detected at the  $N\text{-}\sigma$  level after an integration time  $t_{\text{int}}$ . Suppose we repeat the same observation, but we create a first image by passing the incoming radiation through a linear polarizer for  $0.5t_{\text{int}}$ . Next, we create a second image by observing the remaining  $0.5t_{\text{int}}$  through a linear polarizer that is rotated by 90 degrees compared to the first observation. If one subtracts the two images, then any unpolarized emission is removed down to the level of  $\sim \sigma$ .

## 5 CONCLUSIONS

The high-redshift Universe is known to contain luminous Ly $\alpha$  emitting sources such as galaxies and quasars. The Ly $\alpha$  photons that are emitted by these sources are typically scattered both in the interstellar medium and in the intergalactic medium. In this paper we have calculated polarization properties of this scattered Ly $\alpha$  radiation.

We used a Monte-Carlo Ly $\alpha$  radiative transfer code, and endowed each Ly $\alpha$  photon with a polarization vector which is perpendicular to the photon's wave vector. In this formulation the Stokes parameters resulted from binning together multiple independent photons. We differentiated between resonant and wing scattering, as these are described by different scattering matrices (see Appendix A). Wing scattering is described by classical Rayleigh scattering and in this case we advanced the photon's polarization vector in a scattering event following the well-tested approach of Rybicki & Loeb (1999). However, resonant scattering is described by a superposition of Rayleigh scattering and isotropic scattering with corresponding weights of 1/3 and 2/3 (§ 2.2). In this case, minor modifications to the approach of Rybicki & Loeb (1999) are required when advancing the photon's polarization vector (§ 2.3).

We have applied our code to three classes of models which represent the diverse sets of environments around high-redshift galaxies:

- First, we computed the polarization of the back-scattered Ly $\alpha$  radiation observed from galaxies surrounded by a superwind-driven outflow. We have found that the fractional polarization may reach values as high as  $\mathcal{P}_{\text{max}} \sim 40\%$ , where the maximum polarization depends on parameters such as the speed of the outflow,  $v_{\text{exp}}$ , and the column density of neutral hydrogen atoms,  $N_{\text{HI}}$  (§ 3.1). In this case we have found the polarization to increase towards longer wavelengths.
- Second, we considered resonant scattering in the intergalactic medium (IGM) *after* reionization. Residual intergalactic hydrogen can scatter up to  $\gtrsim 90\%$  of the Ly $\alpha$  emitted by galaxies out of the line of sight. (This high fraction does not apply to galaxies with superwind-driven outflows where the Ly $\alpha$  photons are scattered out of resonance before they encounter the IGM.) We have found the polarization of the scattered Ly $\alpha$  halo around galaxies to be polarized at lower levels ( $\mathcal{P}_{\text{max}} \lesssim 7\%$ ) than the halos around galaxies with

the small angular scales of interest here. Identifying polarized Ly $\alpha$  lines could in principle be optimized by using special purpose filters that search for the circular polarization pattern shown in Figure 2 around the sources of interest.

outflows. This follows from the fact that Ly $\alpha$  photons scatter multiple times when they enter resonance, which isotropizes the local Ly $\alpha$  radiation field and reduces its net polarization. The polarization decreases with the mean number of scattering events the photons experience (i.e. the polarization decreases with an increasing effective optical depth in the Ly $\alpha$  line). For this reason, we expect the polarization of resonantly scattered Ly $\alpha$  photons in the IGM to be largest around low redshift sources or around sources where the IGM is more highly ionized than average (e.g. in the vicinity of a bright quasar, see § 3.2).

- Third, we considered neutral collapsing protogalaxies that are emitting Ly $\alpha$  cooling radiation. Despite the fact that these clouds are extremely optically thick to Ly $\alpha$  photons, and photons typically scatter  $\sim \tau$  times, we found the polarization to linearly increase toward the edge of the cloud, reaching a maximum amplitude of  $\mathcal{P}_{\max} \sim 35\%$ . (§ 3.3). The resulting polarization increases towards shorter wavelengths in contrast to the trend found in outflow models.

Our results indicate that resolved high-redshift Ly $\alpha$  emission may be highly polarized under a variety of likely circumstances. High-redshift Ly $\alpha$  emitters are usually distinguished from low-redshift line emitters on the basis of their broad-band colors and their asymmetric spectral line shape. The work presented here implies that polarization may provide an additional diagnostic. Moreover, polarimetry has the potential to better remove the glow of infrared lines in the Earth's atmosphere, which would improve the sensitivity of ground-based observations to high-redshift Ly $\alpha$  emitting galaxies outside the currently available redshift windows.

The polarization properties of Ly $\alpha$  radiation encode information about the distribution and kinematics of neutral gas in and around galaxies. Polarimetry therefore complements the constraints that are derivable from spectroscopy. From a theorist's perspective, it is therefore well worth to include polarization in calculations of Monte-Carlo codes of Ly $\alpha$  radiative transfer.

The redshifted Ly $\alpha$  line has provided us with an important window into the high-redshift Universe. This work suggests that in order to fully exploit the observations, one should focus on both Stokes parameters  $I$  and  $Q$ , rather than just  $I$ . Polarization measurements to less than 1% accuracy can be carried out by existing facilities such as for example the FOCAL Reducer/low dispersion Spectrograph (FORS1)<sup>5</sup> on the VLT, the LRIS imaging spectropolarimeter at the W.M. Keck Observatory (Goodrich & Cohen 2003), and the CIAO polarimeter on Subaru (Tamura et al. 2003). The results of this paper imply that Ly $\alpha$  emitting objects provide excellent targets.

**Acknowledgments** We thank G. Rybicki & Adam Lidz for useful discussions. This research was supported by Harvard University funds.

## REFERENCES

- Adams, T.F. 1972, ApJ, 174, 439
- Adelberger, K. L., Steidel, C. C., Kollmeier, J. A., & Reddy, N. A. 2006, ApJ, 637, 74
- Ahn, S.-H., Lee, H.-W., & Lee, H. M. 2002, ApJ, 567, 922
- Ahn, S.-H., Lee, H.-W., & Lee, H. M. 2003, MNRAS, 340, 863
- Barkana, R., & Loeb, A. 2003, *Nature*, 421, 341
- Lee, H.-W., & Blandford, R. D. 1997, MNRAS, 288, 19
- Brandt, J. C., & Chamberlain, J. W. 1959, ApJ, 130, 670
- Brasken, M., & Kyrola, E. 1998, A&A, 332, 732
- Cantalupo, S., Porciani, C., Lilly, S. J., & Miniati, F. 2005, ApJ, 628, 61
- Cantalupo, S., Lilly, S. J., & Porciani, C. 2007, ApJ, 657, 135
- Chambers, K. C., Miley, G. K., & van Breugel, W. J. M. 1990, ApJ, 363, 21
- Chandrasekhar, S. 1960, New York: Dover, 1960,
- Dijkstra, M., Haiman, Z., & Spaans, M. 2006, ApJ, 649, 14
- Dijkstra, M., & Wyithe, J. S. B. 2007, MNRAS, 379, 1589
- Dijkstra, M., Wyithe, J. S. B., & Haiman, Z. 2007a, MNRAS, 379, 253
- Dijkstra, M., Lidz, A., & Wyithe, J. S. B. 2007b, MNRAS, 377, 1175
- Fan, X., et al. 2006, AJ, 132, 117
- Fernandez, E. R., & Komatsu, accepted to MNRAS, arXiv:0706.1801
- Furlanetto, S. R., & Loeb, A. 2003, ApJ, 588, 18
- Glass, I. S. 1999, Highlights of Astronomy,
- Goodrich, R. W. 1992, ApJ, 399, 50
- Goodrich, R., & Cohen, M. 2003, Proceedings of SPIE, 4843, 146
- Gould, A., & Weinberg, D. H. 1996, ApJ, 468, 462
- Haiman, Z., & Spaans, M. 1999, ApJ, 518, 138
- Haiman, Z., & Rees, M. J. 2001, ApJ, 556, 87
- Haiman, Z., & Cen, R. 2005, ApJ, 623, 627
- Hamilton, D. R. 1947, ApJ, 106, 457
- Hansen, M., & Oh, S. P. 2006, MNRAS, 367, 979
- Harrington, J. P. 1973, MNRAS, 162, 43
- Hayes, M., Ostlin, G., Atek, H., Kunth, D., Mas-Hesse, J. M., Leitherer, C., Jimenez-Bailon, E., & Adamo, A. 2007, MNRAS in press, archiv/0710.2622
- Horton, A., Parry, I., Bland-Hawthorn, J., Cianci, S., King, D., McMahon, R., & Medlen, S. 2004, Proceedings of the SPIE, 5492, 1022
- Hu, E. M., & McMahon, R. G. 1996, *Nature*, 382, 231
- Hu, E. M., Cowie, L. L., McMahon, R. G., Capak, P., Iwamura, F., Kneib, J.-P., Maihara, T., & Motohara, K. 2002, ApJL, 568, L75
- Ikeda, Y., Akitaya, H., Matsuda, K., Homma, K., Seki, M., Kawabata, K. S., Hirata, R., & Okazaki, A. 2004, ApJ, 604, 357
- Iye, M., et al. 2006, *Nature*, 443, 186
- Kashikawa, N., et al. 2006, ApJ, 648, 7
- Keller, H. U., Richter, K., & Thomas, G. E. 1981, A&A, 102, 415
- Kobayashi, M. A. R., Totani, T., & Nagashima, M. 2007, accepted to ApJ, arXiv:0705.4349
- Kodaira, K., et al. 2003, PASJ, 55, L17
- Kunth, D., Mas-Hesse, J. M., Terlevich, E., Terlevich, R., Lequeux, J., & Fall, S. M. 1998, A&A, 334, 11
- Laursen, P., & Sommer-Larsen, J. 2007, ApJL, 657, L69
- Lee, H. W. 1994, MNRAS, 268, 49
- Lee, H.-W., & Ahn, S.-H. 1998, ApJL, 504, L61
- Lee, H.-W., & Yun, J.-H. 1998, MNRAS, 301, 193
- Loeb, A., & Rybicki, G. B. 1999, ApJ, 524, 527

<sup>5</sup> <http://www.eso.org/instruments/fors/>

Maihara, T., Iwamuro, F., Yamashita, T., Hall, D. N. B., Cowie, L. L., Tokunaga, A. T., & Pickles, A. 1993, *PASP*, 105, 940

Malhotra, S., & Rhoads, J. E. 2002, *ApJL*, 565, L71

Malhotra, S., & Rhoads, J. E. 2004, *ApJL*, 617, L5

Matsuda, Y., et al. 2004, *AJ*, 128, 569

McQuinn, M., Lidz, A., Zahn, O., Dutta, S., Hernquist, L., & Zaldarriaga, M. 2007, *MNRAS*, 377, 1043

Meinel, I. A. B. 1950a, *ApJ*, 111, 555

Meinel, A. B., II 1950b, *ApJ*, 112, 120

Mesinger, A., & Furlanetto, S. 2007, submitted to *MNRAS*, arXiv:0708.0006

Modali, S. B., Brandt, J. C., & Kastner, S. O. 1972, *ApJ*, 175, 265

Mori, M., Umemura, M., & Ferrara, A. 2004, *ApJL*, 613, L97

Neufeld, D. A. 1990, *ApJ*, 350, 216

Nilsson, K. K., Orsi, A., Lacey, C. G., Baugh, C. M., & Thommes, E. 2007, *A&A*, 474, 385

Osterbrock, D. E. 1962, *ApJ*, 135, 195

Ota, K., et al. 2007, submitted to *ApJ*, arXiv:0707.1561

Ouchi, M., et al. 2007, submitted to *ApJ*, arXiv:0707.3161

Partridge, R. B., & Peebles, P. J. E. 1967, *ApJ*, 147, 868

Ramsay, S. K., Mountain, C. M., & Geballe, T. R. 1992, *MNRAS*, 259, 751

Rauch, M., et al. 2007, Accepted to *ApJ*, arXiv:0711.1354

Rhoads, J. E., Malhotra, S., Dey, A., Stern, D., Spinrad, H., & Jannuzi, B. T. 2000, *ApJL*, 545, L85

Rybicki, G. B., & Lightman, A. P. 1979, New York, Wiley-Interscience, 1979. 393 p.,

Rybicki, G. B., & Loeb, A. 1999, *ApJL*, 520, L79

Saito, T., Shimasaku, K., Okamura, S., Ouchi, M., Akiyama, M., & Yoshida, M. 2006, *ApJ*, 648, 54

Santos, M. R. 2004, *MNRAS*, 349, 1137

Schmidt, G. D., & Miller, J. S. 1985, *ApJ*, 290, 517

Schuster, A. 1879, *MNRAS*, 40, 35

Semelin, B., Combes, F., & Baek, S. 2007, *A&A*, 474, 365

Shapley, A. E., Steidel, C. C., Pettini, M., & Adelberger, K. L. 2003, *ApJ*, 588, 65

Spergel, D. N., et al. 2007, *ApJS*, 170, 377

Stanway, E. R., et al. 2007, *MNRAS*, 376, 727

Stark, D. P., Ellis, R. S., Richard, J., Kneib, J.-P., Smith, G. P., & Santos, M. R. 2007a, *ApJ*, 663, 10

Stark, D. P., Loeb, A., & Ellis, R. S. 2007b, *ApJ*, 668, 627

Steidel, C. C., Giavalisco, M., Pettini, M., Dickinson, M., & Adelberger, K. L. 1996, *ApJL*, 462, L17

Steidel, C. C., Adelberger, K. L., Shapley, A. E., Pettini, M., Dickinson, M., & Giavalisco, M. 2000, *ApJ*, 532, 170

Stenflo, J. O. 1980, *A&A*, 84, 68

Tamura, M., Fukagawa, M., Murakawa, K., Suto, H., Itoh, Y., & Doi, Y. 2003, *Proceedings of SPIE*, 4843, 190

Taniguchi, Y., & Shioya, Y. 2000, *ApJL*, 532, L13

Tapken, C., et al. 2006, *A&A*, 455, 145

Tasitsiomi, A. 2006, *ApJ*, 645, 792

Trager, S. C., Faber, S. M., Dressler, A., & Oemler, A. J. 1997, *ApJ*, 485, 92

Verhamme, A., Schaerer, D., & Maselli, A. 2006, *A&A*, 460, 397

Verhamme, A., et al. 2008, in prep.

Weidinger, M., Møller, P., & Fynbo, J. P. U. 2004, *Nature*, 430, 999

Westra, E., et al. 2006, *A&A*, 455, 61

White, H. E. 1934, *Introduction to Atomic Spectra*, International Series in Pure and Applied Physics, Auckland: McGraw-Hill International

Wyithe, J. S. B., & Loeb, A. 2005, *ApJ*, 625, 1

Yoo, J. J., Bak, J.-Y., & Lee, H.-W. 2002, *MNRAS*, 336, 467

Zheng, Z., & Miralda-Escudé, J. 2002, *ApJ*, 578, 33

## APPENDIX A: POLARIZATION OF RESONANTLY SCATTERED $\text{Ly}\alpha$

### A1 $\text{Ly}\alpha$ Scattering Matrix

The scattering matrix for a scattering process that is a superposition of Rayleigh and isotropic scattering of weight  $E_1$  and  $E_2$  may be written as (Chandrasekhar 1960, Eq 250-258)

$$R = \frac{3}{2}E_1 \begin{pmatrix} \cos^2 \theta & 0 \\ 0 & 1 \end{pmatrix} + \frac{1}{2}E_2 \begin{pmatrix} 1 & 1 \\ 1 & 1 \end{pmatrix} \quad (\text{A1})$$

where

$$\begin{pmatrix} I'_l \\ I'_r \end{pmatrix} = R \begin{pmatrix} I_l \\ I_r \end{pmatrix}. \quad (\text{A2})$$

Here,  $I'_l$  and  $I'_r$  are the components of the scattered intensity parallel and perpendicular to the plane of scattering, respectively. If the incoming light is assumed to be unpolarized, then  $I_l = I_r = \frac{1}{2}$ , and the phase function and degree of polarization are given by (Chandrasekhar 1960, Eqs. 250–258)

$$p(\theta) = E_2 + \frac{3}{4}E_1 + \frac{3}{4}E_1 \cos^2 \theta, \quad \Pi(\theta) = \frac{\sin^2 \theta}{1 + \frac{4E_2}{3E_1} + \cos^2 \theta} \quad (\text{A3})$$

Comparison with Eq. (3) reveals that  $\text{Ly}\alpha$  resonant scattering of unpolarized light corresponds to the case  $E_1 = \frac{1}{3}$  and  $E_2 = \frac{2}{3}$ .

As was mentioned in § 2.2, the non-zero degree of polarization arises fully<sup>6</sup> from scattering between the levels  $1S_{1/2} \rightarrow 2P_{3/2} \rightarrow 1S_{1/2}$ . This transition is denoted by H (while K denotes the  $1S_{1/2} \rightarrow 2P_{1/2} \rightarrow 1S_{1/2}$  transition). Hamilton (1947) showed that for the H and K transitions  $(E_1, E_2)_H = (\frac{1}{2}, \frac{1}{2})$  and  $(E_1, E_2)_K = (0, 1)$ . Hence, scattering by  $90^\circ$  via the H-transition results in  $\Pi(90^\circ) = \frac{2}{7}$ , as was already mentioned in § 2.2. Because scattering is twice as likely to occur via the H transition, the scattering averaged value becomes  $(E_1, E_2) = \frac{1}{3}(E_1, E_2)_K + \frac{2}{3}(E_1, E_2)_H = (\frac{1}{3}, \frac{2}{3})$ .

Lastly, we point out that Rayleigh and isotropic scattering by  $90^\circ$  results in 100 and 0% polarization, respectively. Since resonant scattering may be viewed as a superposition of Rayleigh scattering and isotropic scattering with corresponding weights of  $1/3$  and  $2/3$ , one might expect  $90^\circ$  resonant scattering to result in a fractional polarization of  $\frac{1}{3}$ ,

<sup>6</sup> A simple way to see why scattering through the  $2P_{1/2}$  level does not result in any polarization is that the angular part of the wavefunction describing the electron in the  $2P_{1/2}$ -state is a constant (e.g. White 1934, p. 134). Hence an atom that is excited into the  $2P_{1/2}$ -state has ‘lost’ any memory of the direction and/or polarization of the photon that excited the atom. The photon that is emitted when the atom decays back to the ground state has no preferred direction (i.e. it is emitted with an equal probability in all directions).

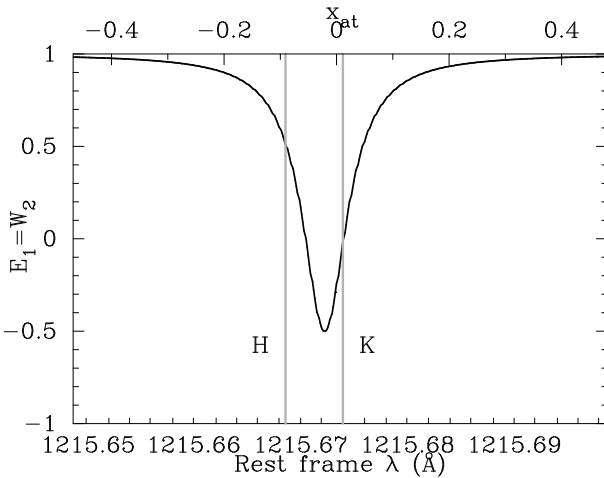


**Figure A1.** The impact of quantum interference on the polarization in resonant Ly $\alpha$  scattering. The frequency dependence of the parameter  $E_1$  (see Eq. A1), as calculated by Stenflo (1980), is shown. One finds  $E_1 = \frac{1}{2}$  and  $E_1 = 0$  at the H and K resonance frequencies as expected. At sufficiently large separations from both resonances,  $E_1 \rightarrow 1$ , which corresponds to pure Rayleigh scattering. Interestingly,  $E_1 < 0$  for a range of frequencies between the H and K resonance frequency. In practice, however, scattering at these frequencies does not occur often enough to leave an observable imprint (see text, and Fig A2). The upper horizontal axis shows frequency in normalized units  $x$  (we arbitrarily set  $x = 0$  at  $\nu = \nu_K$ ).

while the actual number is  $\Pi(90^\circ) = \frac{3}{11} < \frac{1}{3}$ . The main reason for this difference is that isotropic and Rayleigh scattering have different phase functions, and that if scattering by  $90^\circ$  occurs, then the probability that this was due to isotropic scattering is larger than  $\frac{2}{3}$ .

## A2 Quantum Interference as in Stenflo (1980)

In § 2.2 the phase function and the degree of polarization caused by resonant and wing scattering were given. Here we discuss the transition between these two regimes. Stenflo (1980) has calculated the value of  $E_1$  as a function of frequency (but note that  $E_1 = W_2$  in the notation of Stenflo 1980, Eq. 3.25). We have plotted  $E_1$  as a function of wavelength (bottom label) and frequency (top label) in Figure A1.

Figure A1 shows that  $E_1 = \frac{1}{2}$  at the H resonance frequency and  $E_1 = 0$  at the K resonance frequency, which correspond exactly to the values quoted above. The Figure also shows that at sufficiently large separations from both resonances,  $E_1 \rightarrow 1$ . In dimensionless frequency units, this asymptotic value is practically reached when  $|x_{\text{at}}| \gtrsim 0.2$ . This was the motivation for using the threshold  $x_{\text{crit}} = 0.2$  to separate core from wing scattering in § 2.3.

Interestingly,  $E_1 < 0$  for a range of frequencies between the H and K resonance frequencies. However, scattering at these frequencies does not occur often enough to leave an observable imprint. The reason for this is simple: the natural width of the line for both the H and K transitions is much smaller than their separation, i.e.  $\gamma_{\text{H,K}} \sim 10^8 \text{ Hz} \ll \nu_{\text{H}} - \nu_{\text{K}} = 1.1 \times 10^{10} \text{ Hz}$ . Since the absorption cross-section in the atom's rest-frame scales as,  $\sigma(\nu) \propto [(\nu - \nu_{\text{H,K}})^2 + \gamma_{\text{H,K}}^2/4]^{-1}$ , a Ly $\alpha$  photon is much more likely absorbed by an atom for

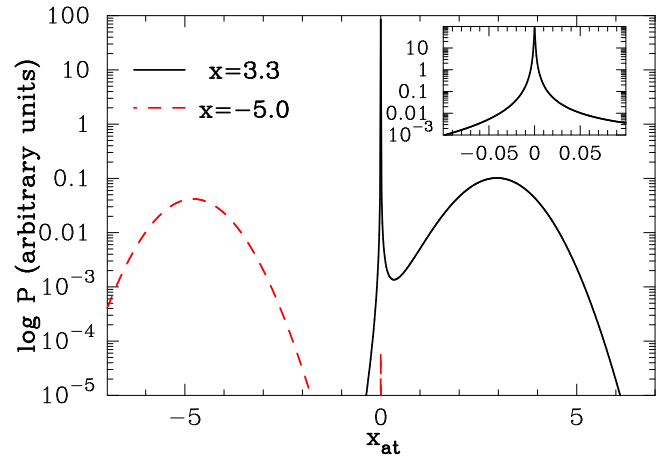


**Figure A2.** The probability that a photon of frequency  $x$  is scattered by an atom such that it appears at a frequency  $x_{\text{at}}$  in the frame of the atom. The *solid* and *dashed* lines correspond to  $x = 3.3$  and  $x = -5.0$  respectively,  $P(x_{\text{at}}, x)$  (Eq. A4). For  $x = 3.3$ , photons are either scattered by atoms to which they appear *exactly* at resonance (see inset), or to which they appear  $\sim 3$  Doppler widths away. For  $x = -5$ , resonant scattering is less important by orders of magnitude. In combination with Fig A1, this figure shows that if a photon is resonantly scattered then  $E_1$  is either 0 or  $\frac{1}{2}$ .

which the photon appears exactly at resonance, than by an atom for which the photon has an energy corresponding to a negative  $W_2$ . Quantitatively, the Maxwellian probability  $P$  that a photon of frequency  $x$  is scattered at frequency  $x_{\text{at}}$  in the atom's rest-frame is given by

$$P(x_{\text{at}}, x) dx_{\text{at}} = \frac{a}{\pi H(a, x)} \frac{e^{-(x_{\text{at}} - x)^2}}{x_{\text{at}}^2 + a^2} dx_{\text{at}}, \quad (\text{A4})$$

where  $H(a, x)$  is the Voigt function ( $H(a, x) \equiv \tau_x/\tau_0$ , see Eq 2). This probability is shown in Figure A2 for  $x = 3.3$  (*solid* line) and  $x = -5.0$  (*dashed* line). Figure A2 shows that for  $x = 3.3$ , photons are scattered either when they are exactly at resonance or when they appear  $\sim 3$  Doppler widths away from resonance. The inset of Figure A2 zooms on the region near  $x_{\text{at}} = 0.0$ . Clearly, if a photon is resonantly scattered, then it is more likely to be scattered when it is *exactly* at resonance than when it is, say, 0.05 Doppler widths away from resonance. For frequencies  $|x| > 3.3$  there are not enough atoms moving at velocities such that the Ly $\alpha$  photon appears at resonance in the frame of the atom. Instead, the photon is scattered while it is in the wing of the absorption profile. This is illustrated by the *dashed* line which shows the case  $x = -5.0$ , for which resonant scattering is less likely by orders of magnitude.

From the above we conclude that (i) when a photon is scattered in the wing of the line profile, then  $E_1 = 1$  and (ii) when a photon is scattered resonantly, then it is scattered almost exactly at resonance, and therefore  $E_1 = \frac{1}{3}$  (the scattering-averaged value).

<sup>7</sup> Note that the transition from core to wing scattering occurs at  $x \sim 3.3$ , see § 2.1.